NASA Technical Memorandum 102709

An Analysis of the Effects of Secondary Reflections on Dual-Frequency Reflectometers

C. P. Hearn
C. R. Cockrell
S. D. Harrah

October 1990

National Aeronautics and Space Administration

Langley Research Center
Hampton, Virginia 23665-5225

AN ANALYSIS OF THE EFFECTS OF SECONDARY REFLECTIONS ON DUAL-FREQUENCY REFLECTOMETERS

Abstract

The problem of secondary reflections in a double-sideband suppressed carrier (DSB-SC) reflectometer (distance measurement) system is examined analytically and the use of carrier-frequency modulation to mitigate the measurement error produced by multiple reflections is demonstrated.

Introduction

This paper is an analysis of the measurement errors caused by spurious reflections in single- and two-frequency continuous-wave ranging systems, the latter of the type originally proposed for the Microwave Reflectometer Ionization Sensor (MRIS). The analysis is purely mathematical and reduced to the simplest level possible for purposes of explanation. It is hoped that these results will be a catalyst and stimulate thought and discussion, and promote analysis which will lead to the development of a better instrument. Details concerning mechanization are purposely ignored here so as to emphasize fundamental concepts. Actual hardware realization can add another dimension of possible problems.

Errors are quantified in terms of the ratio of the desired to the spurious, or undesired, signal amplitudes (C/I or carrier-to-interference ratio) over the unambiguous measurement range of the system. The basis of error reduction by carrier frequency sweeping is explained, and the improvement to be expected is defined. An adaptive sweep technique is proposed which, at this elementary level of analysis, appears promising.

Single-frequency distance measurement

As a preliminary, consider a monochromatic signal exciting a radiating aperture which is large in wavelengths, and therefore, transmits essentially a plane-wave. If a perfectly reflecting plate is located a distance, d, away from the aperture and illuminated, as in figure 1, the complex reflection coefficient is, ideally,

$$\Gamma_{IN} \equiv \frac{V_R}{V_F} = e^{-2\gamma d} = \rho(d)\angle\theta(d) \qquad (1)$$

The phase of Γ_{IN} is

$$\theta(d) = -2\beta d = -4\pi\left(d/\lambda_g\right) = -4\pi d\left(f/c\right) \qquad (2)$$

where β is the imaginary part of the propagation constant, γ. The phase of Γ_{IN} is a linear function of d and has a maximum unambiguous range, d_{MAX}, of $\lambda_g/2$, or $c/2f$, where $\theta(d)$ reaches -2π radians.

Consider the effect of an additional reflection in this system of magnitude, A_0, which is unrelated to the reflecting plate, as in the case of a mismatched antenna. For simplicity, assume that the secondary reflection is independent of frequency, as diagramed in figure 2. The phase angle of Γ_{IN} with these two reflections is

$$\theta_R = \tan^{-1}\left(\frac{A_1 \operatorname{Sin}\theta_1}{A_0 + A_1 \operatorname{Cos}\theta_1}\right) = \tan^{-1}\left[\frac{\operatorname{Sin}\theta_1}{\left(A_0/A_1\right) + \operatorname{Cos}\theta_1}\right] \qquad (3)$$

which is clearly not a linear function of the phase angle of the primary return, θ_1, and hence, d. Figure 3 is a sketch of the resultant phase, θ_R, with $A_0 > 0$ (solid) and $A_0 = 0$ (dotted). The maximum phase deviation from the $A_0 = 0$ case is $\arctan(A_0/A_1)$ which occurs when the components of the received signal are in phase-quadrature.

Dual-frequency distance measurement

In the MRIS mission, scientific requirements, dictating that the excitation frequency exceed 20 GHz and the measurement range extend out to 15 cm, rule out a single-frequency approach. To satisfy these requirements, two signals are transmitted, such that at the maximum range the phase difference between the two signals equals 2π radians. From (2), this phase difference is

$$\theta_D \equiv \theta_U - \theta_L = -\left(4\pi d/\lambda_U\right) + \left(4\pi d/\lambda_L\right) = -4\pi d\left(f_U - f_L\right)/c \qquad (4)$$

which is the same phase angle that would result from a single tone at the difference frequency ($f_U - f_L$) transmitted in a nondispersive (constant time delay at all frequencies) medium.

The effect of a secondary reflection is considered just as in the single-frequency case, except that two frequencies are involved. Figure 4 is a polar depiction of the two phasor components of the received signal at the two frequencies, and figure 5 is a plot of the phase angles at each frequency as a function of d. Note that the unambiguous range is much greater than for either of the signals alone. The net phase angle at each frequency can be written by inspection; however, we choose to find the deviation of the net phase from the phase with $A_0 = 0$. This means that deviation of the sum vector from the primary return is sought. By inspection,

$$\Delta\theta_i = \tan^{-1}\left(\frac{A_0 \operatorname{Sin}(-\theta_i)}{A_1 + A_0 \operatorname{Cos}(-\theta_i)}\right) \qquad i = U \text{ or } L \qquad (5)$$

The total phase error, $\Delta\theta_T$, is the difference between $\Delta\theta_U$ and $\Delta\theta_L$, or

$$\Delta\theta_T = -\tan^{-1}\left(\frac{\left(A_0/A_1\right)\operatorname{Sin}\theta_U}{1 + \left(A_0/A_1\right)\operatorname{Cos}\theta_U}\right) + \tan^{-1}\left(\frac{\left(A_0/A_1\right)\operatorname{Sin}\theta_L}{1 + \left(A_0/A_1\right)\operatorname{Cos}\theta_L}\right) \qquad (6)$$

When $A_0/A_1 \ll 1$, each component of $\Delta\theta_T$ has a maximum value of approximately $\arctan(A_0/A_1)$; however, since θ_U and θ_L can, by design, differ by up to 2π radians, the total differential phase error can be twice that at each frequency. Equation (6), while exact, is not intuitively satisfying. Such a relationship can be derived if it is assumed that $A_0/A_1 < 0.1$, in which case (6) can be closely approximated as

$$\Delta\theta_T \simeq -\left(\frac{A_0}{A_1}\right)\operatorname{Sin}\theta_U\left[1 - \left(\frac{A_0}{A_1}\right)\operatorname{Cos}\theta_U\right] + \left(\frac{A_0}{A_1}\right)\operatorname{Sin}\theta_L\left[1 - \left(\frac{A_0}{A_1}\right)\operatorname{Cos}\theta_L\right] \qquad (7)$$

Using the identity $\operatorname{Sin} 2\theta = 2(\operatorname{Sin}\theta \cdot \operatorname{Cos}\theta)$ in (7) gives

$$\Delta\theta_T \simeq -\left(\frac{A_0}{A_1}\right)\left(\operatorname{Sin}\theta_U - \operatorname{Sin}\theta_L\right) + \left(\frac{A_0}{A_1}\right)^2\left(\frac{\operatorname{Sin} 2\theta_U - \operatorname{Sin} 2\theta_L}{2}\right) \qquad (8)$$

Using function-difference identities in (8) gives

$$\Delta\theta_T \simeq -2\left(\frac{A_0}{A_1}\right)\text{Cos}\left(\frac{\theta_U + \theta_L}{2}\right)\cdot\text{Sin}\left(\frac{\theta_U - \theta_L}{2}\right) + \left(\frac{A_0}{A_1}\right)^2\text{Cos}\,(\theta_U + \theta_L)\cdot\text{Sin}\,(\theta_U - \theta_L) \qquad (9)$$

Using (4) in (9) leads to

$$\Delta\theta_T \simeq -2\left(\frac{A_0}{A_1}\right)\text{Cos}\,(2\omega_o d/c)\cdot\text{Sin}\,((\omega_U - \omega_L)d/c) + \left(\frac{A_0}{A_1}\right)^2\text{Cos}\,(4\omega_o d/c)\cdot\text{Sin}\,(2(\omega_U - \omega_L)d/c) \qquad (10)$$

where ω_o is defined as $\omega_o \equiv (\omega_U + \omega_L)/2$.

It can be seen that the (approximate) $\Delta\theta_D(d)$ has a rapidly-varying component, Cos $(2\omega_o d/c)$, with a slowly-varying envelope, Sin $((\omega_U - \omega_L)d/c)$, and harmonics thereof. The sine term can be expressed as Sin $(2\omega_M d/c)$ since the sideband spacing resulting from the product of a (sinusoidal) carrier and a modulation signal is twice the modulation frequency, and $(\omega_U - \omega_L) = 2\omega_M$. Making use of this fact and (4) allows (10) to be expressed as

$$\Delta\theta_T \simeq -2\left(\frac{A_0}{A_1}\right)\text{Cos}\left(\pi\left(\frac{f_o}{f_M}\right)\left(\frac{d}{d_{MAX}}\right)\right)\cdot\text{Sin}\left(\pi\left(\frac{d}{d_{MAX}}\right)\right) + \left(\frac{A_0}{A_1}\right)^2\text{Cos}\left(2\pi\left(\frac{f_o}{f_M}\right)\left(\frac{d}{d_{MAX}}\right)\right)\cdot\text{Sin}\left(2\pi\left(\frac{d}{d_{MAX}}\right)\right) \qquad (11)$$

which is useful for studying the behavior of $\Delta\theta_T$ with d.

Figure 6 is a sketch of the total differential phase, θ_D, which includes the first error term in (10), which is dominant when $A_0/A_1 < 0.1$, and the desired component given by (4). Upon comparison with figure 3, it is seen that the regions of maximum error on (0, d_{MAX}) are different with respect to the maximum unambiguous range, but carrier-frequency ripple is present in both cases.

As noted earlier, for a given C/I, the two-frequency system has a maximum phase error twice that of a single-frequency system.

Path-length dependent spurious reflections

Another type of spurious reflection is path-length dependent, as diagramed in figure 7 with only one multiple reflection. The phase angle of the first multiple reflection is always twice that of the primary return. Following the same procedure as before, the phase deviation at each frequency can be written as

$$\Delta\theta_I = \tan^{-1}\left[\frac{A_0 \text{ Sin } (2\omega_I d/c)}{A_1 + \text{Cos } (2\omega_I d/c)}\right] \qquad \text{for } I = U \text{ or } L \qquad (12)$$

and the total phase error is

$$\Delta\theta_T \equiv \Delta\theta_U - \Delta\theta_L =$$

$$\tan^{-1}\left[\frac{\left(\frac{A_0}{A_1}\right)\text{Sin } (2\omega_U d/c)}{1 + \left(\frac{A_0}{A_1}\right)\text{Cos } (2\omega_U d/c)}\right] - \tan^{-1}\left[\frac{\left(\frac{A_0}{A_1}\right)\text{Sin } (2\omega_L d/c)}{1 + \left(\frac{A_0}{A_1}\right)\text{Cos } (2\omega_L d/c)}\right] \qquad (13)$$

Upon comparison of (13) and (6), it is seen that the phase error resulting from path-dependent spurious reflections is out of phase with that caused by path-independent reflections. This is because the differential phase shifts between the spurious and primary reflections are of different senses in the two cases.

Swept-frequency averaging

The error-producing effects of secondary reflections can be significantly reduced by sweeping the carrier frequency while holding the separation between the two sidebands constant. The underlying basis of this error-reduction technique can be demonstrated most simply with a single-frequency example. Figure 8 is an extension of figure 3, plotting the sum-vector phase angle, θ_R, as a function of d for three frequencies: $\omega_o - \Delta\omega/2$, ω_o and $\omega_o + \Delta\omega/2$. With d fixed at d_o, and the secondary reflections frequency-invariant, the phase error can range between $\pm\arctan[A_0/A_1]$, as shown in figure 8. If the total frequency excursion is large enough to rotate the primary reflection, from d_o, through exactly 2π radians, the error will average to zero. To achieve a 2π radian variation, the frequency in (2) would have to be shifted by

$$\Delta f\Big|_{2\pi} = c/2d_o \qquad (14)$$

Thus, there is a minimum range at which a $\pm\pi$ radian variation can be achieved with a symmetrical frequency sweep. It is easily concluded from figure 3 that this minimum range is $d_{MAX}/2$, and the required frequency sweep ($\Delta\omega$) is from 0 to $2\omega_o$! Such a wide fractional frequency sweep is obviously impractical, especially in waveguide hardware; however, if in a two-frequency system the sideband spacing is small compared to the carrier frequency, or $(f_U - f_L) << (f_U + f_L)/2$, the percentage Δf required to provide meaningful error reduction is much smaller, and the technique becomes feasible. The rapidly-varying term in (10) is required to go through at least 2π radians as f_o is swept, hence

$$(\Delta f)_{MIN} > c/2d_{MIN} \qquad (15)$$

independent of f_o. It is making f_o so large that the ratio $(\Delta f)_{MIN}/f_o$ becomes small, rather than the value of f_o itself, that makes implementation feasible.

Consider now the application of carrier sweeping in a nonadaptive manner to reduce error. The differential phase error after averaging (10) over $\Delta\omega$ is by definition:

$$\overline{\Delta\theta_T} \equiv \frac{1}{\Delta\omega}\int_{\omega_o - \Delta\omega/2}^{\omega_o + \Delta\omega/2} \Delta\theta_T(\omega,\omega_M)\, d\omega \qquad (16)$$

When $A_0/A_1 < 0.1$, this integration yields

$$\overline{\Delta\theta_T} = -2\left(\frac{A_0}{A_1}\right)\left[\frac{\mathrm{Sin}\ (\Delta\omega d/c)}{\Delta\omega d/c}\right]\mathrm{Sin}(2\omega_M d/c)\mathrm{Cos}(2\omega_o d/c) \qquad (17)$$

for the first and dominant term in (16). Upon comparison with (11), the effective error reduction factor is seen to be of the well known form

$$\text{Sinc}\ (\Delta\omega d/c) \equiv \left[\frac{\text{Sin}\ (\Delta\omega d/c)}{\Delta\omega d/c}\right] \tag{18}$$

An obvious first choice for $\Delta\omega$ would be to pick it so that the first zero of the Sinc function occurs where the unswept error in (10), and figure 6, would be maximum, at $d = d_{MAX}/2$. Using (4), the $\Delta\omega$ required to make $\Delta\omega d/c = \pi$ at $d_{MAX}/2$ is $\Delta\omega = 4\omega_M$. Figure 9 (solid trace) is a plot of (18) with this value of $\Delta\omega$. When $d > d_{MAX}/2$, the error is reduced by a factor of at least 0.212 (-13.4 dB); however, there is little error reduction when $d << d_{MAX}/2$. From this it is concluded that $\Delta\omega$ should be selected to make the argument of (18) equal π at the minimum measurement range (dotted trace for the case $d_{MIN} = d_{MAX}/6$). In general

$$\Delta f = 2f_M \cdot \left(\frac{d_{MAX}}{d_{MIN}}\right) \tag{19}$$

The maximum possible value of (17) is $2(A_0/A_1)$; the averaged error envelope normalized to this factor is plotted in figure 10 versus d for $\Delta\omega = 4\omega_M$ and $12\omega_M$, resulting in worst-case normalized envelope magnitudes of 0.44 (-7.1 dB) and 0.16 (-15.9 dB), respectively.

Adaptive error reduction

This approach consists of adapting the carrier sweep width ($\Delta\omega$) so that the argument of the Sinc function always equals π, and the function equals zero. If $\hat{d}$ is the measured value of d, $\Delta\omega$ is controlled so that

$$\Delta f = c/\hat{d} \qquad (20)$$

A reasonable initialization procedure would be to start with the maximum $\Delta\omega$ - to guarantee some error reduction - and then reduce $\Delta\omega$ to satisfy (20), followed by continuous updating. The first zero in figure 9 is "tracked" along with d. For example, the solid trace in figure 10 would correspond to $\hat{d} = d_{MAX}/2$ and the dotted trace to $\hat{d} = d_{MAX}/6$.

Conclusions

Despite the elementary and idealized nature of this analysis, it is believed that the results are applicable to one of the major technical problems confronting the MRIS project; specifically, reflections from the Thermal Protection System (TSP) tile. The results of this analysis can be summarized as follows:

(1) In two-frequency ranging, the maximum measurement error due to spurious reflections is twice that of a single-frequency system, for equal C/I ratios.

(2) Carrier-frequency averaging can reduce errors caused by spurious reflections beyond some minimum range, which is inversely proportional to the sweep width.

(3) Adaptive carrier sweeping can in principle completely eliminate reflection-type errors at distances exceeding d_{MIN}.

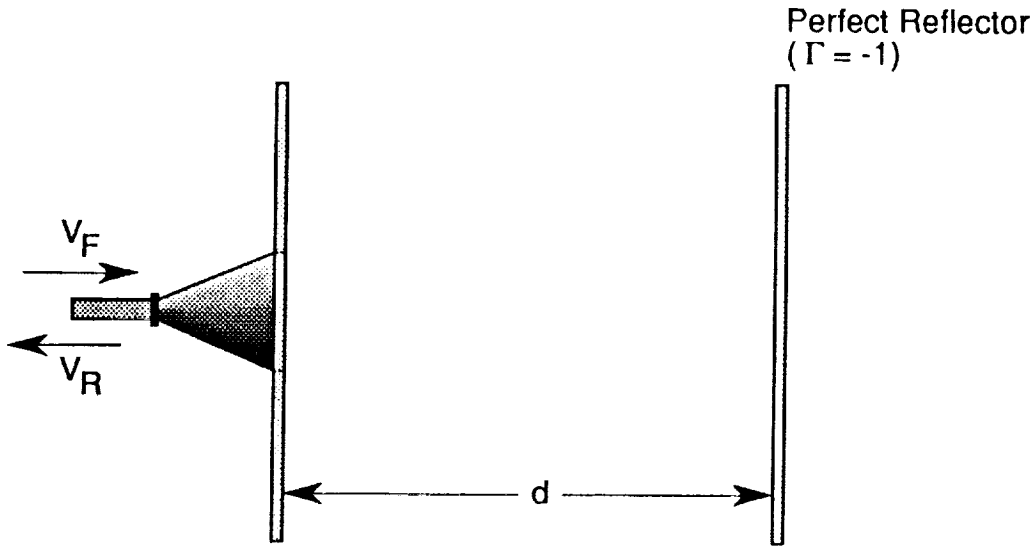

Figure 1.-Large aperture illuminating a flat plate.

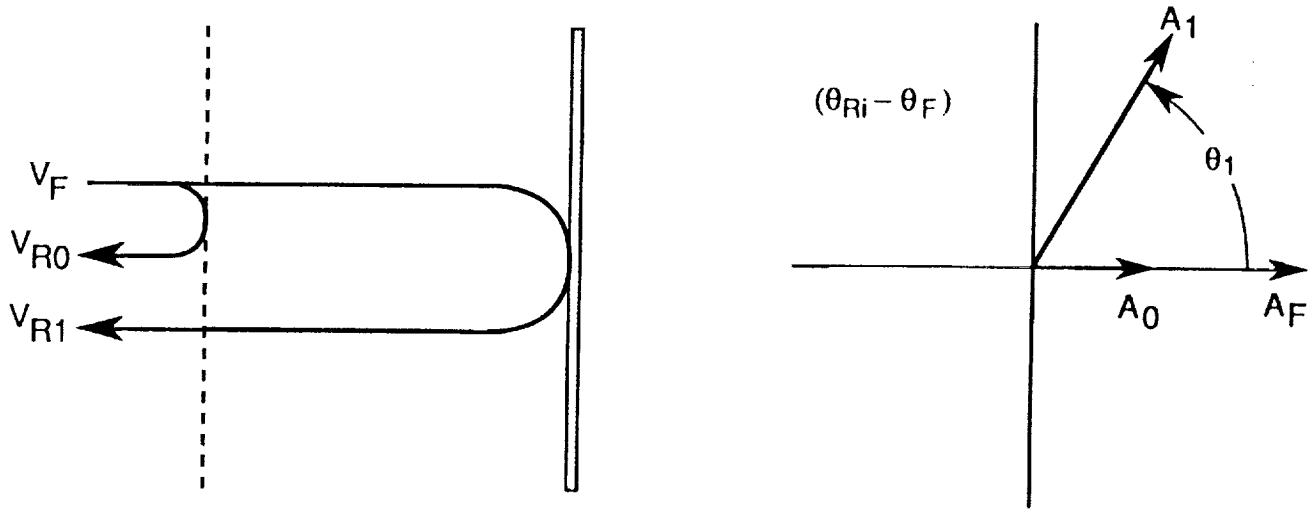

(a) Physical model

(b) Polar diagram, ω reference

Figure 2.-Continuous wave ranging with one secondary reflection.

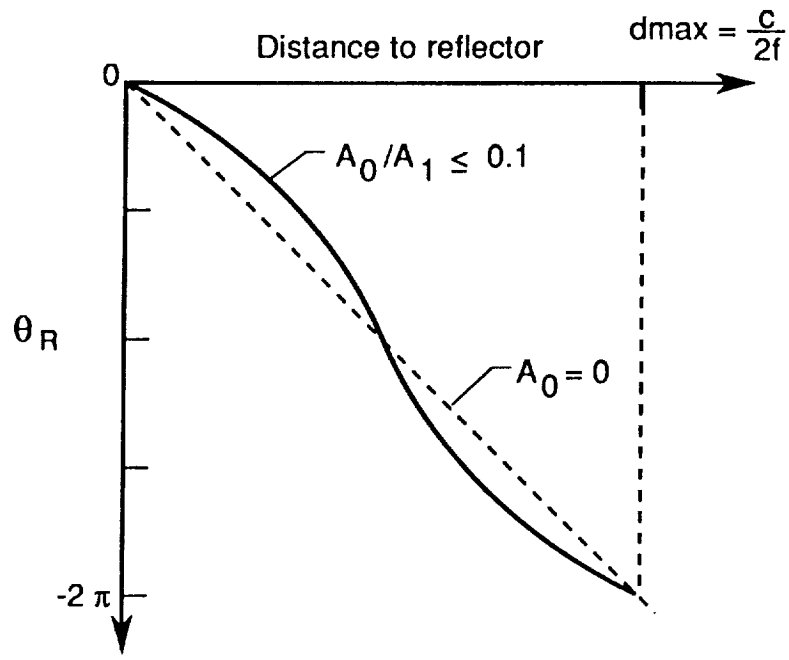

Figure 3.-Sum vector phase as a function of distance-to-reflector.

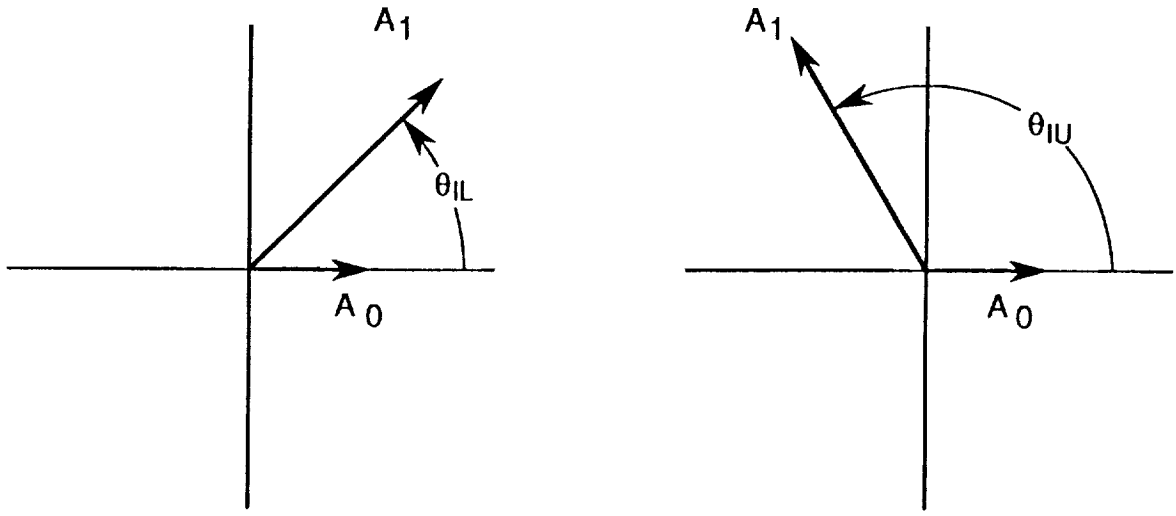

(a) ω_L reference (b) ω_U reference

Figure 4.-Two-frequency ranging with a frequency-invariant spurious reflection.

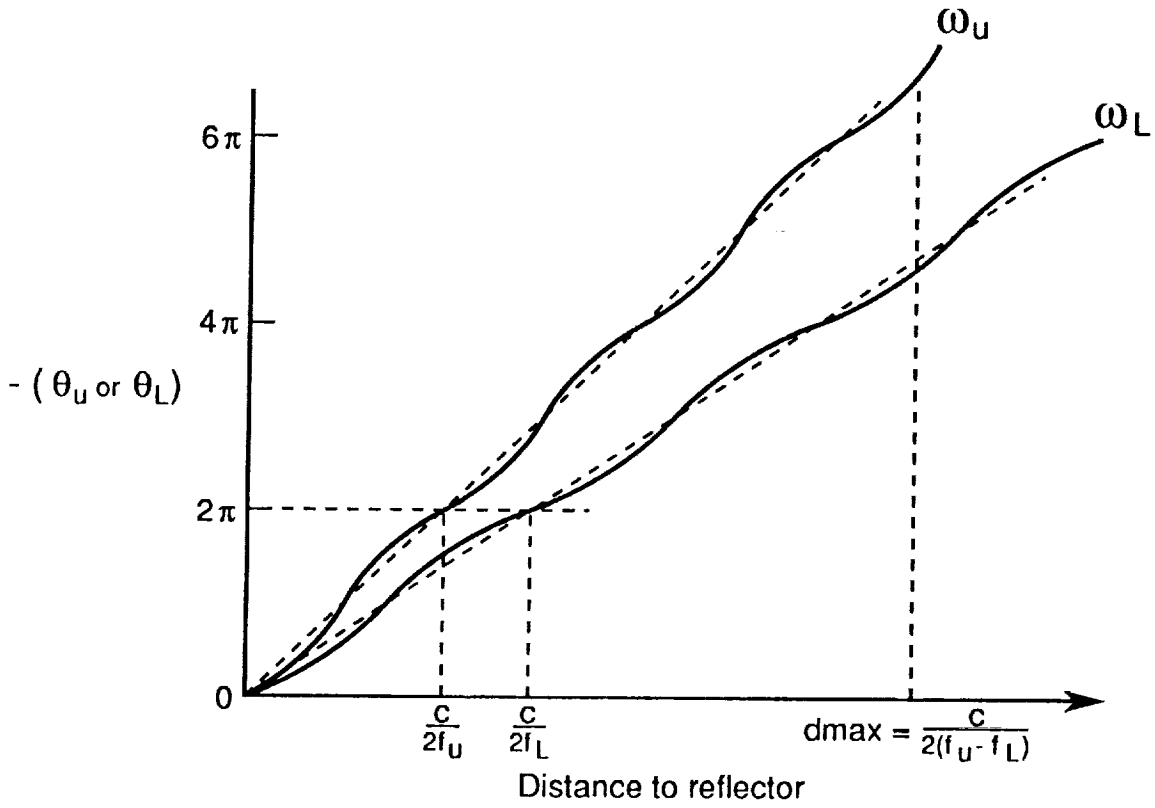

Figure 5.-Phase versus distance for two-frequency system.

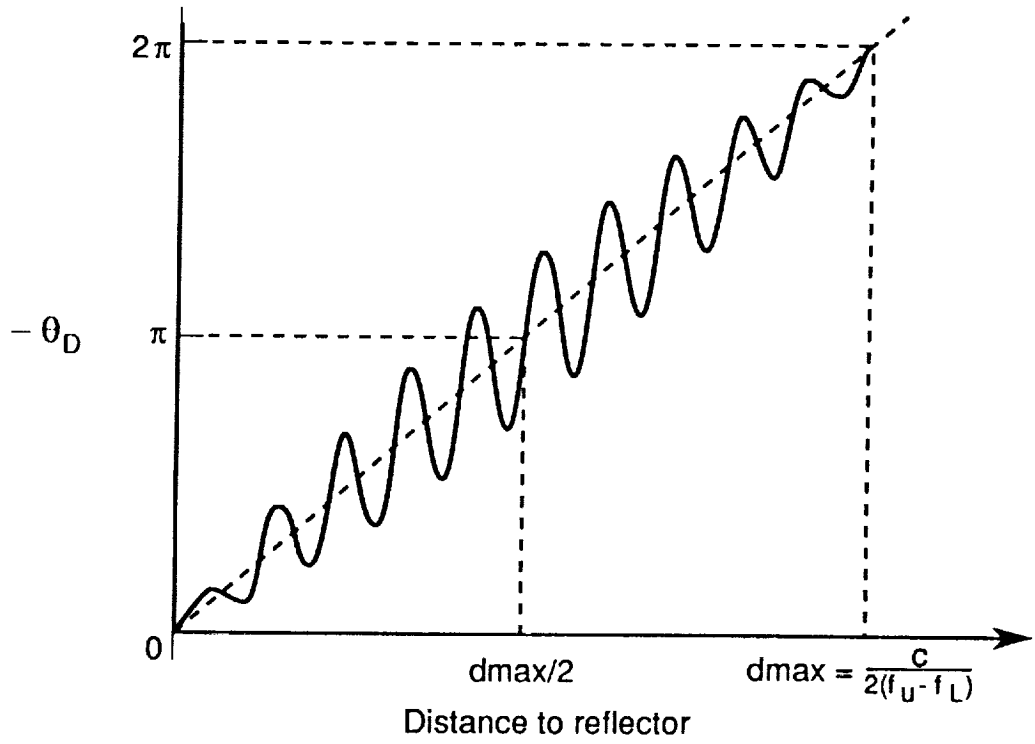

Figure 6.-Phase difference in dual-frequency ranging with a frequency-invariant spurious reflection.

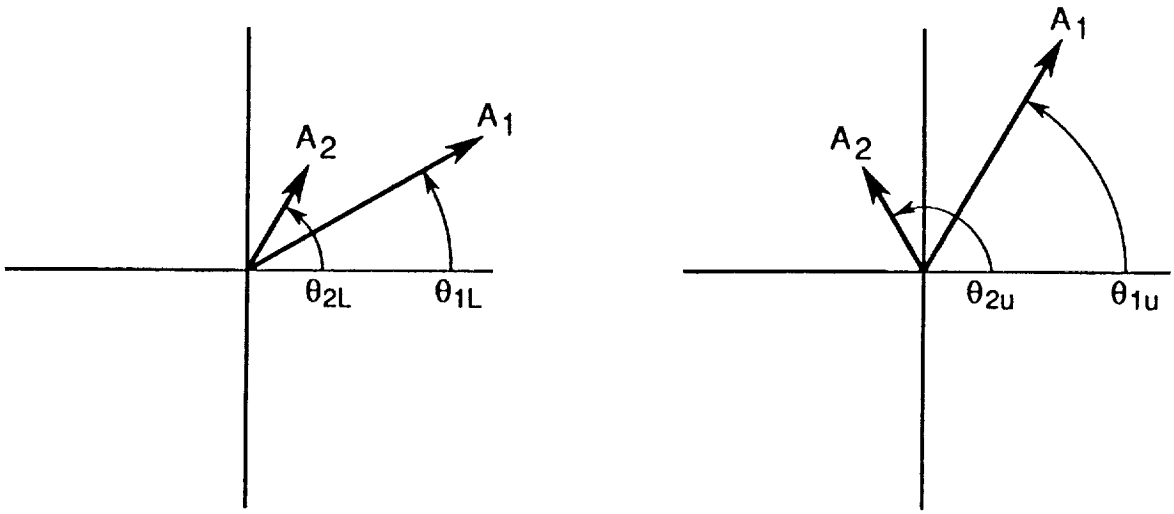

(a) ω_L reference (b) ω_u reference

Figure 7.-Dual-frequency ranging with a path-length-dependant spurious reflection ($\theta_2 = 2\theta_1$).

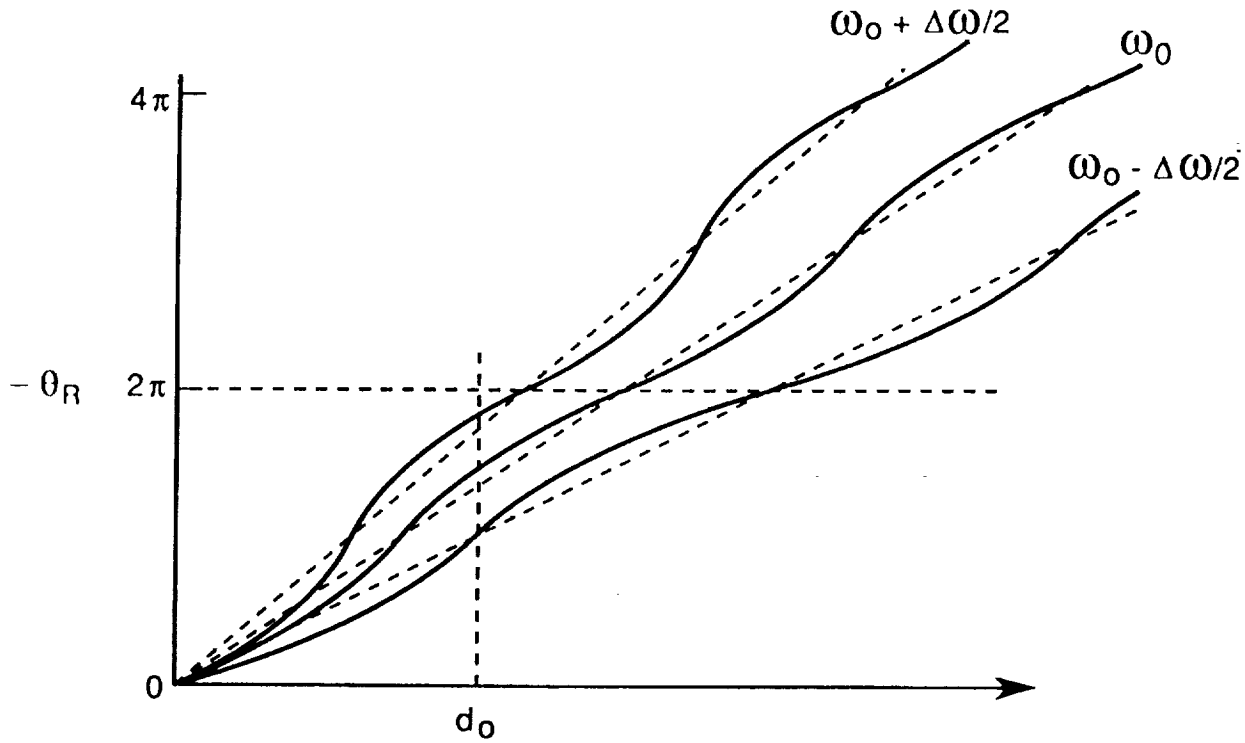

Figure 8.-The effect of frequency-shift on the phase error produced by secondary reflections.

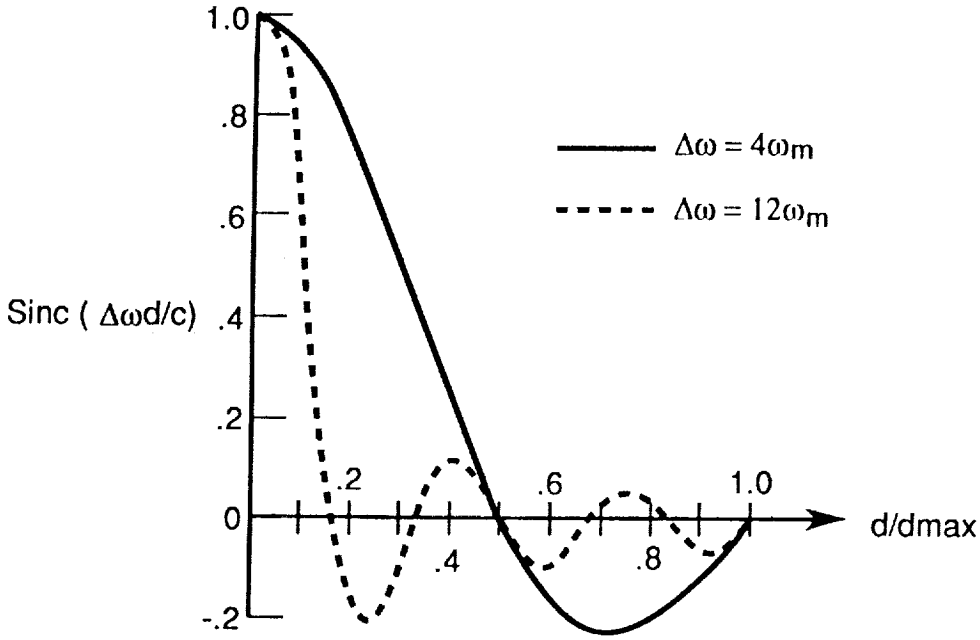

Figure 9.-Error reduction factor vs. distance for different sweep widths.

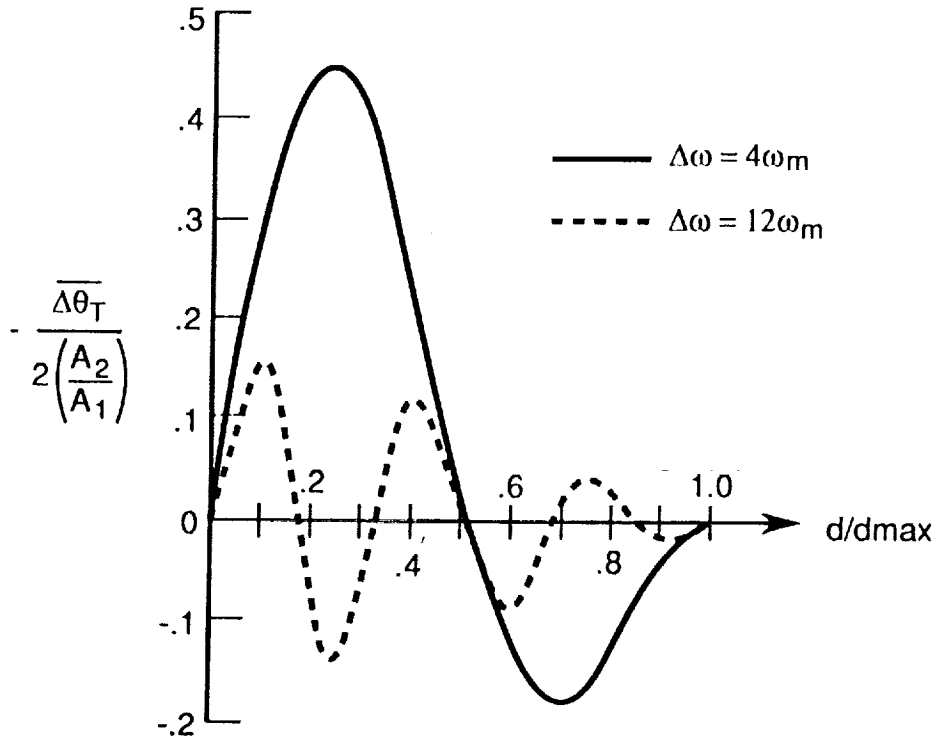

Figure 10.-Normalized phase-error envelope after frequency-averaging.

NASA
National Aeronautics and Space Administration

Report Documentation Page

1. Report No.	2. Government Accession No.	3. Recipient's Catalog No.
NASA TM-102709		

4. Title and Subtitle	5. Report Date
An Analysis of the Effects of Secondary Reflections on Dual-Frequency Reflectometers	October 1990
	6. Performing Organization Code

7. Author(s)	8. Performing Organization Report No.
C. P. Hearn C. R. Cockrell S. D. Harrah	
	10. Work Unit No. 506-44-21-03

9. Performing Organization Name and Address	11. Contract or Grant No.
NASA Langley Research Center Hampton, Virginia 23665-5225	
	13. Type of Report and Period Covered Technical Memorandum

12. Sponsoring Agency Name and Address	14. Sponsoring Agency Code
National Aeronautics and Space Administration Washington, DC 20546-0001	

15. Supplementary Notes

16. Abstract

The error-producing mechanism involving secondary reflections in a dual-frequency, distance-measuring reflectometer is examined analytically. Equations defining the phase, and hence distance, error are derived. The error-reducing potential of frequency-sweeping is demonstrated. It is shown that a single spurious return can be completely nullified by optimizing the sweep width.

17. Key Words (Suggested by Author(s))	18. Distribution Statement
reflectometer, distance measurement error	unclassified - unlimited subject category 33

19. Security Classif. (of this report)	20. Security Classif. (of this page)	21. No. of pages	22. Price
unclassified	unclassified	16	A03